GEOPHYSICS, VOL. 77, NO. 3 (MAY-JUNE 2012); P. O1–O19, 16 FIGS., 1 TABLE.
10.1190/GEO2011-0340.1

Fast probabilistic petrophysical mapping of reservoirs from 3D seismic data

Mohammad S. Shahraeeni[1], Andrew Curtis[2], and Gabriel Chao[3]

ABSTRACT

A fast probabilistic inversion method for 3D petrophysical property prediction from inverted prestack seismic data has been developed and tested on a real data set. The inversion objective is to estimate the joint probability density function (PDF) of model vectors consisting of porosity, clay content, and water saturation components at each point in the reservoir, from data vectors with compressional- and shear-wave-impedance components that are obtained from the inversion of seismic data. The proposed inversion method is based on mixture density network (MDN), which is trained by a given set of training samples, and provides an estimate of the joint posterior PDF's of the model parameters for any given data point. This method is much more time and memory efficient than conventional nonlinear inversion methods. The training data set is constructed using nonlinear petrophysical forward relations and includes different sources of uncertainty in the inverse problem such as variations in effective pressure, bulk modulus and density of hydrocarbon, and random noise in recorded data. Results showed that the standard deviations of all model parameters were reduced after inversion, which shows that the inversion process provides information about all parameters. The reduction of uncertainty in water saturation was smaller than that for porosity or clay content; nevertheless the maximum of the a posteriori (MAP) of model PDF clearly showed the boundary between brine saturated and oil saturated rocks at wellbores. The MAP estimates of different model parameters show the lateral and vertical continuity of these boundaries. Errors in the MAP estimate of different model parameters can be reduced using more accurate petrophysical forward relations. This fast, probabilistic, nonlinear inversion method can be applied to invert large seismic cubes for petrophysical parameters on a standard desktop computer.

INTRODUCTION

Prediction of rock and fluid properties such as porosity, clay content, and water saturation is essential for exploration and development of hydrocarbon reservoirs. Rock and fluid property maps obtained from such predictions can be used in exploration, appraisal, or development of hydrocarbon reservoirs. Seismic data are usually the only source of information available throughout a field that can be used to predict the 3D distribution of properties with appropriate spatial resolution. The main challenge in inferring properties from seismic data is the ambiguous nature of geophysical information. Uncertainty enters into the problem in at least three levels: First, there is nonuniqueness in the inversion of (AVO) seismic data for the acoustic impedances of rock, second, there is nonuniqueness in the petrophysical inversion of the rock impedances for rock-fluid properties given a petrophysical relationship between the acoustic properties and rock-fluid properties, and third, there is ambiguity in these petrophysical relationships themselves (Doyen, 1988). Therefore, any estimate of rock and fluid property maps derived from seismic data must also represent its associated uncertainty.

Rock physics theories are used to construct the petrophysical relations that provide the link between seismic data and reservoir rock properties. Theoretically, elastic moduli and density of rocks are controlled by different rock properties including porosity, clay content, fluid saturations, effective pressure, fluid densities, fluid and

Manuscript received by the Editor 12 September 2011; revised manuscript received 28 December 2011; published online 5 April 2012.
[1]Formerly University of Edinburgh, Edinburgh, U. K.; presently Total E&P U. K., Geoscience Research Centre, Aberdeen, U. K. E-mail: mohammad.shaharaeeni@total.com.
[2]University of Edinburgh and Edinburgh Collaborative of Subsurface Science and Engineering (ECOSSE), Edinburgh, U. K. E-mail: andrew.curtis@ed.ac.uk.
[3]Total E&P France, Geoscience Research Centre, France. E-mail: Gabriel.Chao@total.com.

mineral elastic moduli, and possibly more parameters (Avseth et al., 2005; Mavko et al., 2009). Although some theories and laws appear to be approximately true in many examples of similar specific rock settings, it is very difficult to address effects of all of microscale heterogeneity of rocks in any single set of petrophysical relations. In practice for any particular geologic basin, petrophysical relations are therefore semiempirical, are calibrated with well logs and core data, and their theoretical uncertainty remains nonnegligible (Bachrach, 2006).

Statistical rock physics has been used as a general tool to address uncertainties associated with the petrophysical relations. Mukerji et al. (2001), Avseth et al. (2001), Eidsvik et al. (2004), Buland et al. (2008), and Gonzalez et al. (2008) demonstrate applications of statistical rock physics to estimate lithology units, pay zones, and fluid types from seismic attributes. The Monte Carlo (MC) method (Sambridge and Mosegaard, 2002; Malinverno and Parker, 2006) has also been used to explore all ranges of rock and fluid properties and to simulate elastic responses associated with different petrophysical forward relations. Bosch et al. (2007) show a quantitative application of the MC sampling techniques to obtain compressional impedance and porosity from short-offset seismic data. Bosch et al. (2009) extend their previous work to estimate water saturation in addition to the above two parameters and constrains the final result by geostatistical information from well logs. Spikes et al. (2007) show another application of the MC sampling to invert two constant-angle stacks of seismic data for porosity, clay content, and water saturation in an exploration setting. Bachrach (2006) applies MC sampling to produce porosity and water saturation maps from seismic compressional- and shear-impedance. Sengupta and Bachrach (2007) also apply MC sampling to estimate reservoir pay volume with its associated uncertainty from seismic data. Grana and Della Rossa (2010) apply a sampling algorithm to produce a priori joint PDF of porosity, clay content, water saturation, and compressional- and shear-wave impedance using petrophysical forward relations and a priori information about litho-fluid classes at wellbores. Using the above joint PDF, they estimate the joint PDF of porosity, clay content, and water saturation conditioned on seismic compressional- and shear-wave impedance. In this way, they propagate uncertainty from seismic data to petrophysical parameters in a Bayesian approach. Bosch et al. (2010) provide a general introduction about applications of MC sampling in seismic inversion for reservoir properties.

Although in principle, the MC sampling method can map uncertainty of petrophysical parameters, in practice, applying it to invert seismic attributes for rock and fluid properties can be extremely computationally demanding. For each point in the subsurface, the forward problem (in this case the petrophysical relationships) must be evaluated for a large number of model samples (typically at least of the order of thousands), and this process would have to be repeated for all data points of interest in a seismic cube, which usually includes hundreds of millions of data points. In addition, storing the obtained probabilistic results (many MC samples per data point) can require large storage facilities. Consequently, efficient application of MC sampling techniques requires large computational facilities and is usually implemented on a small subset of the available data points.

As a solution, we present a mixture density network (MDN) as a new tool for probabilistic inversion of seismic attributes to obtain rock and fluid properties. The MDN provides a solution to the time and the memory problems associated with the MC sampling method. Previously, Devilee et al. (1999) and Meier et al. (2007a, 2007b; 2009) show other geophysical applications of the MDN for solving 1D inverse problems. The latter papers invert global seismological data sets for the global distribution of various rock properties and structures in the crust and upper mantle, showing that large, seismic-like data sets can be inverted efficiently and probabilistically for 3D earth models. Shahraeeni and Curtis (2009, 2011) used the MDN to invert acoustic velocity logs for porosity and clay content profiles down wellbores, showing that the method can be used for probabilistic inversion of well logs.

Neural networks have also been used to classify lithofacies successions from borehole well logs. Maiti et al. (2007) and Maiti and Tiwari (2009) apply neural networks to identify lithofacies boundaries using density, neutron porosity, and gamma ray logs of the German Continental Deep Drilling Project (KTB). However, these two papers did not address the problem of inverting data for the joint PDF of a continuous multidimensional model vector, as in Devilee et al. (1999), Meier et al. (2007a, 2007b; 2009), and Shahraeeni and Curtis (2009, 2011). Hampson et al. (2001) and Schultz et al. (1994) also apply neural networks to predict log properties from seismic data. They discuss several practical aspects of application of neural networks for prediction of log properties. In addition to neural networks, other methods of automatic data integration are also applied in the seismic reservoir modeling. For example, Eftekharifar and Han (2011) apply unsupervised clustering and principal component analysis (PCA) for modeling of reservoir rock properties from seismic attributes. For other background information, Poulton (2002) provides a detailed description of mathematical theory and other geophysical applications of neural networks.

In this paper, we jointly invert industrial seismic compressional and shear impedances for the joint probability density function (PDF) of porosity, clay content, and water saturation, using calibrated petrophysical relations and other prior information from wells. The resulting property maps are obtained from the integration of geophysical information, well logs, and rock physics information in an exploration setting. In the same way as Bachrach (2006) and Spikes et al. (2007), in this study information about vertical and spatial geologic continuity has been incorporated in the process of seismic inversion for elastic impedances, and hence, indirectly constrains the final property maps.

First, we briefly present the MDN method of solving an inverse problem, and then introduce petrophysical forward relations, a priori information about model parameters, and data uncertainties. The statistical behavior of the petrophysical forward relations due to a priori uncertainty of model parameters and noise in data are then analyzed. After analysis of the forward function, the inversion results are presented. This is followed by a discussion about results, and conclusions.

THEORY

Mixture density network solution of an inverse problem

The solution to any inverse problem is a definition of the extent to which any combination of model parameter values are consistent with data, given the data uncertainty. In mathematical terms the solution can be expressed as (Tarantola, 2005):

$$\sigma_M(\mathbf{m}|\mathbf{d}) = K\rho_M(\mathbf{m})L(\mathbf{f}(\mathbf{m})|\mathbf{d}). \quad (1)$$

In this equation, $\mathbf{m}$ is the model parameter vector, $\mathbf{f}$ is the forward function which is assumed to be known and calculable, ρ_M is the a priori PDF of the model vector over the model parameter space M, and σ_M is the a posteriori PDF of the model vector, which represents the solution of the inverse problem and is normalized by constant K. The likelihood function L measures the consistency of a model vector $\mathbf{m}$ with measured data $\mathbf{d}$. It represents the uncertainty of the synthetic data $\mathbf{f}(\mathbf{m})$ due to different sources such as theoretical uncertainties in the forward function $\mathbf{f}$, and also accounts for measurement uncertainties in data $\mathbf{d}$ (the vertical line represents the fact that data $\mathbf{d}$ are measured and hence have fixed values). Equation 1 represents a Bayesian solution because it combines information known prior to inversion, $\rho_M(\mathbf{m})$, with information from a new data set, $L(\mathbf{f}(\mathbf{m})|\mathrm{d})$, using Bayes rule for combining probabilities.

The mixture density network (MDN) is trained to emulate $\sigma_M(\mathbf{m}|\mathbf{d})$ for any measured data $\mathbf{d}$. This is achieved using pairs of a priori samples of model and data vector $(\mathbf{m}, \mathbf{d})$. The set of sample pairs is called a training data set and is constructed in the following way: samples $\mathbf{m}_i$, $i = 1, \ldots, N$, are taken according to the a priori model PDF ρ_M, and for each sample, the corresponding synthetic data $\mathbf{f}(\mathbf{m}_i)$ are calculated. Several samples, $\varepsilon_{i,j}$, $j = 1, \ldots, R$, of data measurement uncertainty, as well as of the theoretical uncertainty in the forward function $\mathbf{f}$ (both of which are represented within the likelihood function L), are added to each calculated synthetic data vector $\mathbf{f}(\mathbf{m}_i)$. This results in several samples of possible measured data vectors $\mathbf{d}$ for each sample of the model vector $\mathbf{m}$: $\{(\mathbf{m}_i, \mathbf{f}(\mathbf{m}_i) + \varepsilon_{i,j}) : i = 1, \ldots, N; j = 1, \ldots, R\}$. Using these samples of pairs, which for short we denote $(\mathbf{m}_k, \mathbf{d}_k)$, $k = 1, \ldots, NR$, the network is trained to map any data vector including its uncertainty into an estimate of the corresponding a posteriori PDF of model vector $\mathbf{m}$. Shahraeeni and Curtis (2011) show that the estimated a posteriori PDF is an approximation of the MC sampled a posteriori PDF of model parameters. A more detailed description of the MDN is given in Appendix A.

Petrophysical forward relations, a priori model PDF, and data uncertainty

We applied the MDN inversion method to invert compressional and shear-wave impedances derived from seismic data, for porosity, clay content, and water saturation in a deep offshore field in Africa. In this section, we describe the petrophysical forward relations, a priori information about model parameters, and the seismic data and its uncertainty.

Petrophysical forward function

The petrophysical forward relations are a combination of Gassmann's law to account for fluid substitution, a mixing law to account for mixed lithology (sand and shale), and empirical depth trend curves to describe pressure effects on the bulk and shear moduli of reservoir rocks. The components of the output vector of this petrophysical relation $\mathbf{d}$ are estimated compressional- and shear-wave impedances, $\mathbf{d} = (I_\mathrm{P}, I_\mathrm{S})$; the input vector is $\mathbf{m}' = (\phi_e, V_{cL}, s_w, p_e, K_{hc}, K_w, \rho_{hc}, \rho_w)$ where ϕ_e is effective porosity, which is defined as the void space outside of porous clay in a unit volume of rock, V_{cl} is clay content, s_w is water saturation, p_e is effective pressure, K_{hc} and K_w are bulk modulus of hydrocarbon and brine, and ρ_{hc} and ρ_w are density of hydrocarbon and brine, respectively. A detailed description of the rock physics model is given in Appendix B. This model is developed for a reservoir with a laminated sand-shale mixture. We do not advocate it as a general model to be used elsewhere. Instead we note that the MDN inversion method on which we focus here can be used to invert any assumed rock physics model. The one in Appendix B should, therefore, be regarded in general as one possibility among many others (for another example, see Shahraeeni and Curtis, 2011).

Figure 1 shows the petrophysical forward function predictions and measured values of P- and S-wave impedances at one well

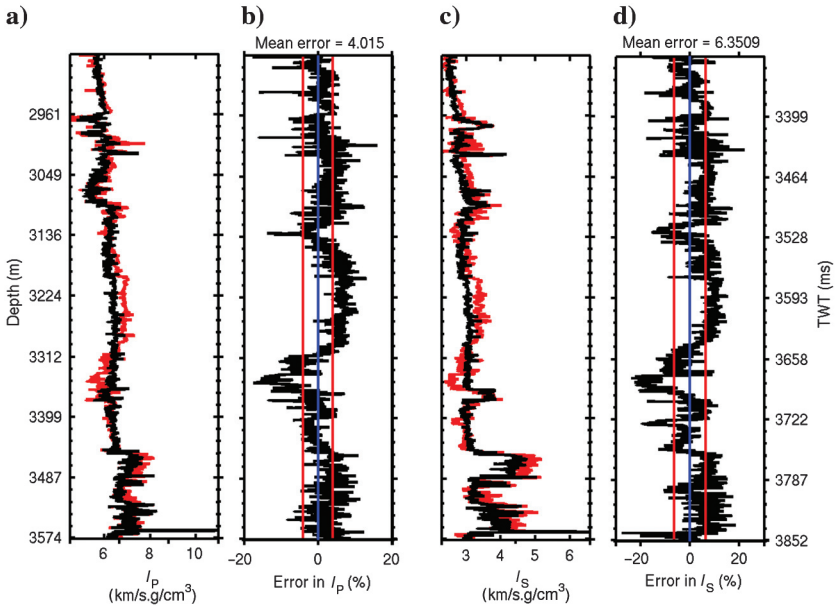

Figure 1. Comparison between prediction of the petrophysical forward function and measured logs and their correlation coefficients (R). (a) Compressional impedance I_P ($R = 0.87$), red curve is the measured log and black curve is the prediction of the petrophysical forward function. (b) Error in I_P (i.e., difference between measured and predicted impedance divided by measured impedance.). Red lines represent two absolute mean error intervals around zero (blue line). (c) Shear-wave impedance I_S ($R = 0.91$). (d) Error in I_S.

in the field. In that figure errors in the prediction of the petrophysical forward function are also shown. The error of the forward function for I_p is around 4% and for I_s is around 6%. However, in some intervals, we observe a bias in the prediction of the petrophysical forward function (e.g., 3154–3295 m and 3312–3367 m). It seems that on these intervals the petrophysical forward function predictions has a systematic error, which may indicate that the selected forward function in Appendix B is not able to model the elastic behavior of rock on these intervals. The effect of these errors on the petrophysical inversion result will be discussed in the "Discussion" section.

Figure 2 shows crossplots of impedances and effective porosity color coded by clay content for samples from the well in Figure 1. The predictions of the petrophysical forward function for water saturated samples at average effective pressure of the well and for different values of clay content are shown by black curves in that figure. These crossplots in addition to error plots in Figure 1 show that in general the petrophysical forward function is able to model the elastic behavior of rocks at the well. However, effect of errors and uncertainties in the predictions of the petrophysical forward function must be taken into account in the petrophysical inversion.

In our inverse problem, the data vector $\mathbf{d} = (I_P, I_S)$ is derived from the inversion of seismic data, and is inverted for the marginal joint PDF of the model vector with porosity, clay content, and water saturation as its components, $\mathbf{m} = (\phi_e, V_{cl}, s_w)$. Other input parameters of the petrophysical forward relations are treated as confounding parameters, $\mathbf{m}_{\text{conf}} = (P_e, K_{hc}, K_w, \rho_{hc}, \rho_w)$ — parameters that may vary and thus alter the uncertainty in estimated model vector $\mathbf{m}$. In mathematical terms, in the MDN solution the confounding petrophysical parameters are integrated out in the marginal a posteriori PDF of the model vector $\mathbf{m}$:

$$\sigma_M(\mathbf{m}|\mathbf{d}) = \int_{\mathbf{m}_{\text{conf}}} \sigma_M(\mathbf{m}'|\mathbf{d})\, d\mathbf{m}_{\text{conf}}. \qquad (2)$$

Thus, the effect of possible variations of confounding model parameters on the posterior PDF is integrated out, and this integration results in an increase in uncertainty of the estimated a posteriori model vector $\mathbf{m} = (\phi_e, V_{cl}, s_w)$.

Seismic data

A 3D simultaneous elastic inversion technique jointly inverted near-, mid-, and far-angle substacks to derive estimates of the 3D distribution of compressional- and shear-wave impedances, I_P and I_S. Five angle stacks were used as the input seismic data

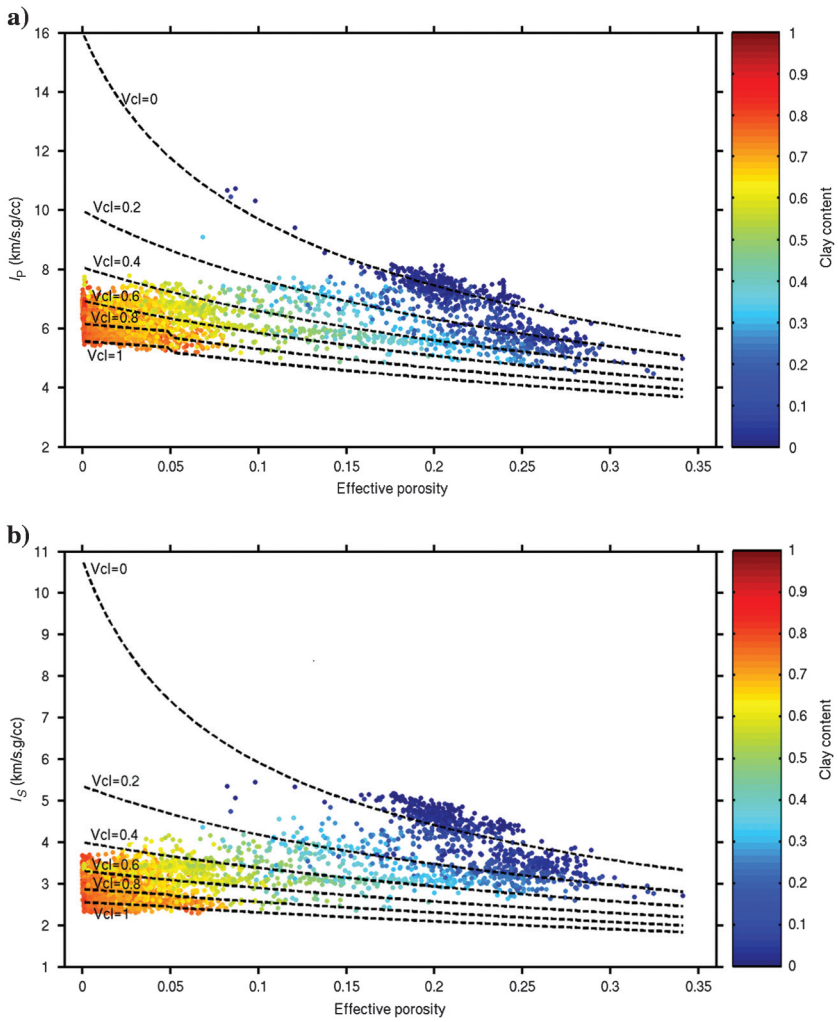

Figure 2. Crossplot of impedances and porosity for samples from one well. (a) Compressional impedance I_P versus effective porosity. Hot colors represent higher values of clay content. Black curves represent predictions of the petrophysical forward function for 100% water saturated samples at the mean effective pressure of the reservoir. (b) Shear-wave impedance I_S versus effective porosity.

set, with angle ranges 0°–13° for near, 13°–21° and 21°–29° for middle, 29°–37° for far, and 37°–45° for ultra-far stacks. The sampling interval of the seismic data was 3 ms. The wavelet for each angle stack was estimated at four different well locations using reflection coefficients obtained from V_P, V_S, and density logs.

Structural and stratigraphic interpretations resulted in picks of 18 different horizons in the seismic data to define the geometry of the initial model used for inversion. The a priori models for I_P and I_S in each horizon were provided by the low-frequency trend of the well logs and were extrapolated over the entire model using kriging methods. The trend of a priori I_P and I_S were obtained from seismic interval velocity (provided from seismic imaging) and the distribution of the residuals was obtained from kriging of well logs (Dubrule, 2003, p. 3–39). The range of the variogram used for the kriging was defined based on a priori geologic information in each of the 18 different horizons of the model geometry. The result of the kriging was then filtered with a low-pass filter (below seismic band-pass) and transferred into the model geometry as prior I_P and I_S model. Finally, An iterative algorithm, based on the simulated annealing technique (Sen and Stoffa, 1991) was used to adjust this prior model estimates of I_P and I_S in each bin, to optimize the match between the input seismic data and the synthetic seismic response calculated by the Zoeppritz equations (Aki and Richards, 1997).

In this way, the seismic-inversion technique combined geologic information about the expected vertical and spatial continuity of the medium, well-log data, and information from seismic data to provide an estimate of the distribution of I_P and I_S. The result for one section, which includes one of the wells, is shown in Figure 3.

Uncertainty of the estimated values of I_P and I_S can be derived either directly from the inversion algorithm (Buland et al., 2003; Buland and Omre, 2003) or by statistical comparison between upscaled I_P and I_S values derived from well-log and seismic-inversion results (Bachrach, 2006). In this study, the latter method was applied and the a posteriori uncertainty of the inversion for I_P was modeled as a Gaussian distribution with zero mean and standard deviation of $\sigma_{I_P} = 0.06\, I_P$, and for I_S was modeled as a Gaussian distribution with zero mean and standard deviation of $\sigma_{I_S} = 0.08\, I_S$. This uncertainty means that if we take several samples of I_P with an average value equal to 6000, 68% of the samples will be between 5640 and 6360. It is important to note that application of this method to estimate uncertainty means that I_P and I_S derived from seismic inversion are assumed to be unbiased. This assumption may be violated where the low-frequency background model used in inversion is biased. In particular, areas of the field with low-effective stress would be bypassed by low-frequency background trend. However, in the area under study in this paper abnormal pressure behavior is not reported and the low-frequency

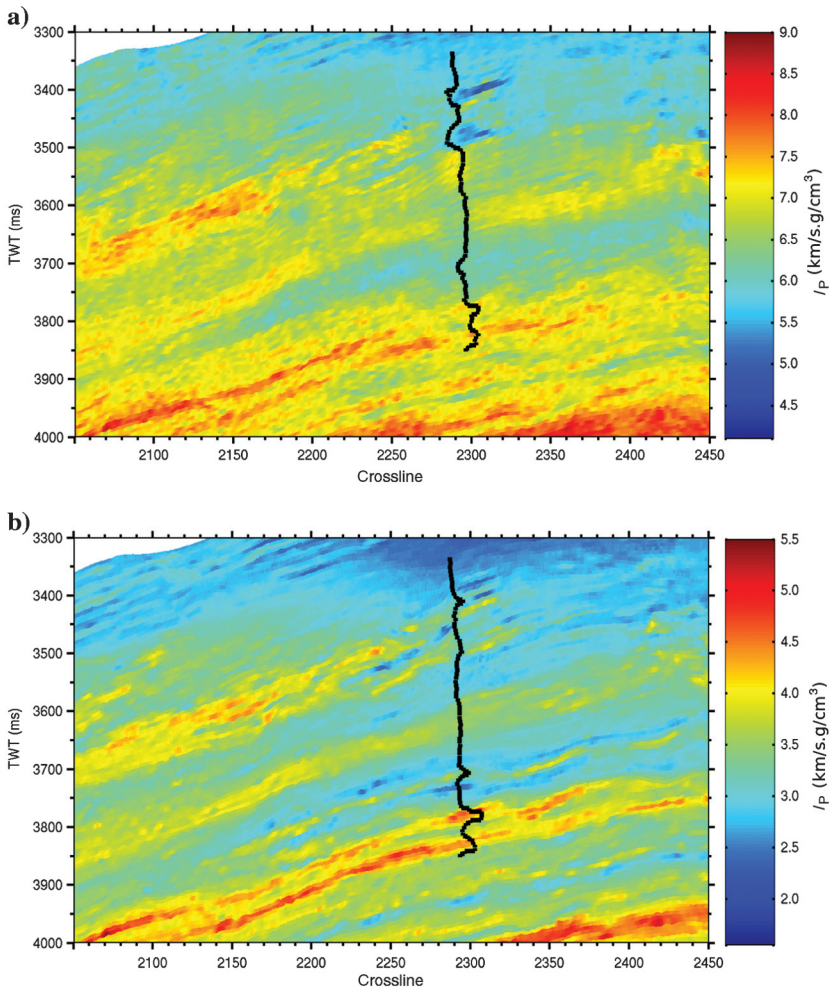

Figure 3. The P- and S-wave-impedance for one cross section of the 3D seismic data set. (a) Compressional-wave impedance. The correlation between inverted samples and upsclaed well logs is $R = 0.88$. (b) Shear-wave impedance ($R = 0.85$). Black curve is the upscaled measured well log.

trend is valid. In general, due to the fact that the statistical estimation of uncertainty is based on well data, it can be an underestimation of the true uncertainty away from the well.

A priori PDF of the input parameters of the forward petrophysical function

To choose the a priori PDF of the model parameters, well-log data from the five wells in the field were analyzed. Figure 4a shows the values of effective porosity versus clay content for well-log samples from the five wells. A correlation between these two parameters can be observed in that figure. Based on this observation, the a priori maximum allowable range or interval for effective porosity and clay content was defined as the region $T(\phi_e, V_{cl})$, which is shown in Figure 4a. Figure 4b and 4c shows effective porosity versus water saturation, and clay content versus water saturation for well-log samples, respectively. These two figures show that, while effective porosity and clay content values are to some extent correlated with water saturation values, there are no hard boundaries to intervals in which parameters lie as there are in Figure 4a. In addition, we observe that for all samples with clay content values higher than 0.8, the water saturation is equal to one. According to these observations we assumed a priori that porosity and clay content were uniformly distributed over the T-area in Figure 4a. Also, we assumed that a priori water saturation is equal to one when clay content is higher than 80%, and that it is uniformly distributed over the [0,1] interval for clay content values lower than 80%. We thus assumed very weak prior information about the three parameters of interest.

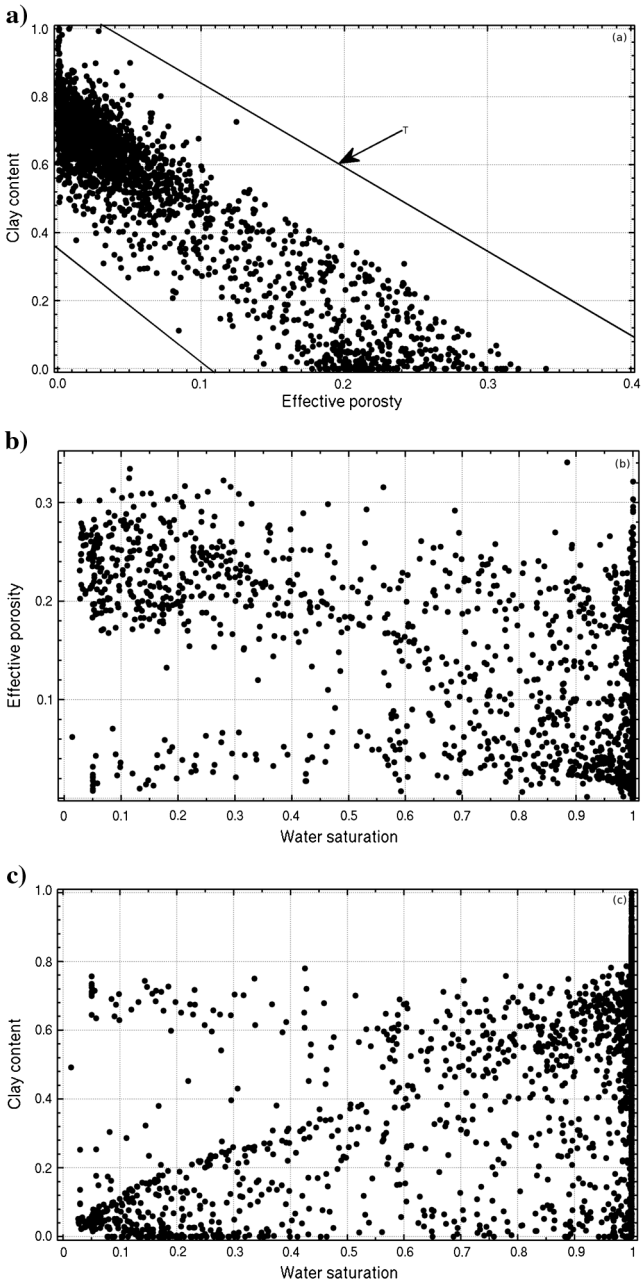

Figure 4. Crossplot of the parameters of the model vector. (a) Clay content versus effective porosity; T represents the a priori region of the porosity-clay content plane. (b) Effective porosity versus water saturation. (c) Clay content versus water saturation.

Effective pressure changes between 173 and 332 bars in the depth intervals that we considered. We do not observe any correlation between effective pressure and effective porosity, clay content, or water saturation in our data set. However, according to Batzle and Wang (1992), the bulk modulus and density of any type of hydrocarbon (with a given value of API degree) are empirical functions of pore pressure and temperature. The pore pressure and overburden stress and hence the effective pressure are assumed to be hydrostatic. The empirical relation between bulk modulus (or density) of fluid and pore pressure is transformed into a relation between bulk modulus (or density) of fluid and effective pressure, using the above assumption. Five different types of hydrocarbon, with different API degrees, were observed in the well intervals we considered. For each type, the bulk modulus as a function of effective pressure, and density as a function of effective pressure, are derived from Batzle and Wang (1992) equations and hydrostatic assumption, and shown in Figure 5a and 5b, respectively. The effect of change of temperature over the interval of interest on both the hydrocarbon bulk modulus and density was assumed to be negligible in this study. Brine density and bulk modulus are equal to 1.008 g/cm^3 and 2.625 GPa, respectively, and are constant in all well intervals we considered. Based on the above observations, effective pressure was assumed to be uniformly distributed between 173 and 223 bar, and bulk modulus and density of fluid were derived from effective pressure using the straight lines in Figure 5 for each of the five different types of hydrocarbon.

The above a priori probability densities are selected to be as noninformative (conservative) as possible given the known constraints. However, they limit possible values of the model parameters to physically realizable values in the field in this study. The MDN inversion method can be applied with any a priori PDF and the above a priori PDF's are selected because they are more suitable for the data in this study.

Forward modeling of I_P: Effect of confounding parameters and uncertainties

In this section, we study the effect of variations of the confounding parameters and measurement uncertainties on the predictions of the petrophysical forward function. Figure 6a shows I_P as a

function of porosity, when all other input parameters of the petrophysical forward relations are held constant at possible realistic values: $V_{cl} = 0.2$, $s_w = 0.3$, $p_e = 200$ bar, $K_{hc} = 0.22$ GPa, $K_w = 2.62$ GPa, $\rho_{hc} = 0.47\,\mathrm{g/cm^3}$, and $\rho_{hc} = 1.008\,\mathrm{g/cm^3}$. The uncertainty in Figure 6a is Gaussian and due to two sources: (1) Uncertainty in the inverted value of I_P and I_S (i.e., measurement uncertainty) and (2) uncertainty in the predictions of the petrophysical forward function (i.e., theoretical uncertainty). The PDF of uncertainty in the inverted value of seismic I_P and I_S is Gaussian and is introduced in the section of seismic data above. The PDF of uncertainty in the predictions of the petrophysical forward function is also Gaussian and introduced in Appendix B. The total uncertainty, which is shown in Figure 6a and 6b is the combined effect of the above two sources of uncertainty. The PDF of this uncertainty is Gaussian and its covariance matrix is equal to the sum of covariance matrices of the above sources of uncertainty (Tarantola, 2005, p. 35). Notice that these plots are different from plots that represent the theoretical uncertainty alone, as might be found in other papers (e.g., Tarantola and Valette, 1982). This is because in the MDN inversion methodology, data measurement uncertainties are also added to the theoretical forward equations uncertainties (Devilee et al., 1999; Meier et al., 2007b; Shahraeeni and Curtis, 2011).

Figure 6b shows I_P as a function of porosity for the constant values of clay content and water saturation given above, but when the confounding parameters (i.e., effective pressure, bulk modulus, and density of hydrocarbon) are varied according to their a priori distributions. The thicker black and dark gray area in Figure 6b in comparison with Figure 6a shows that the uncertainty of the prediction of the petrophysical forward function increases due to variations in the confounding parameters.

Figure 6c, 6d, 6e, and 6f shows variation of I_P as a function of clay content and water saturation in the same manner as Figure 6a and 6b for porosity. In particular, Figure 6d and 6f shows the effect of variations in the confounding parameters on the uncertainty of I_P.

Figure 7 shows a cross section of I_P-ϕ_e for porosity equal to 15%. Different Gaussians in that figure correspond to uncertainty in I_P due to different values of the confounding parameters (in particular effective pressure). Note that due to theoretical relationship between

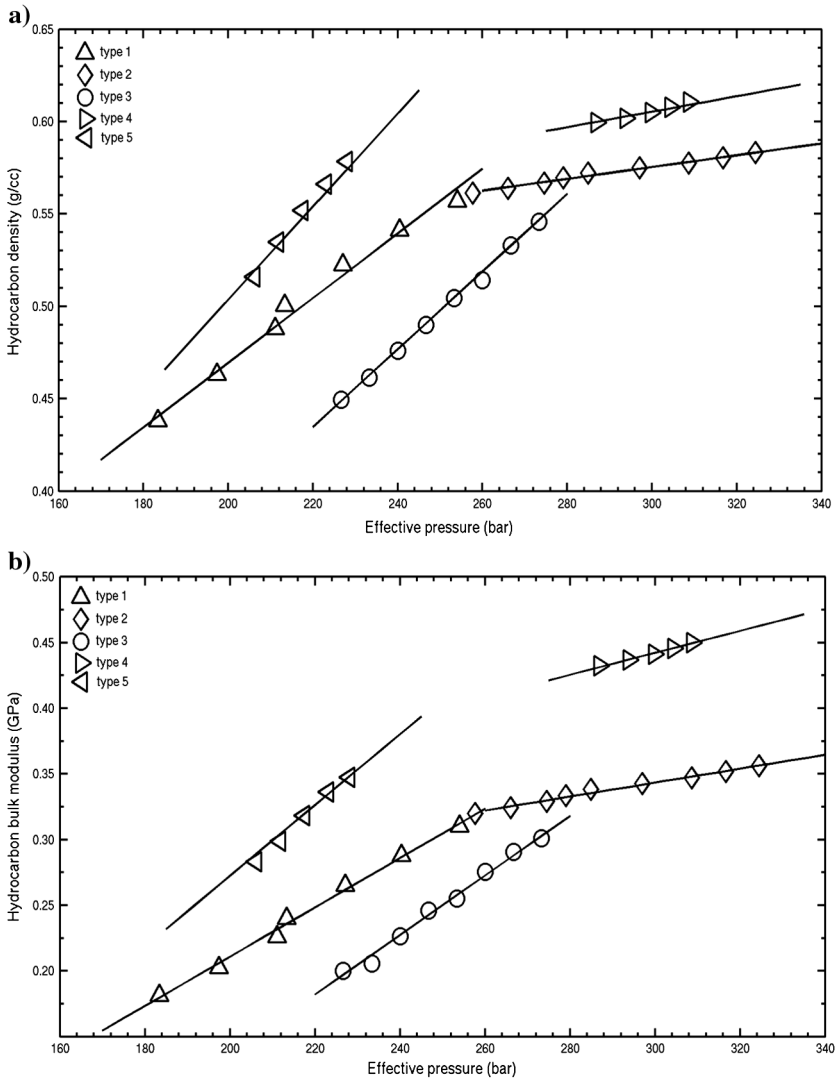

Figure 5. Properties of five different types of hydrocarbons (with different API degrees) in the wells. (a) Density as a function of effective pressure. (b) Bulk modulus as a function of effective pressure.

effective pressure and P- and S-wave impedance, changes in confounding model parameters induce a shift in the mean value of the Gaussians. The black curve represents the sum of different Gaussians and total uncertainty due to uncertainty in the value of confounding parameters, measurement uncertainty and uncertainty in the petrophysical forward function predictions.

Figure 6 shows that although I_P is a strongly varying function of porosity and clay content, and a weakly varying function of water saturation, inference of the petrophysical parameter values from I_P estimates may well be obscured by the high uncertainty of I_P due to uncertainty in the seismic processing, and due to confounding parameters of the petrophysical forward relations. In the same manner as for I_P, uncertainty in I_S is also high due to aforementioned sources and the inference of petrophysical parameters from I_S may also be well obscured. Therefore, with only two data (I_P and I_S) for three unknowns (porosity, clay content, and water saturation) we clearly do not expect a unique solution. Hence, herein we aim principally to assess how much information the seismic data provides to reduce

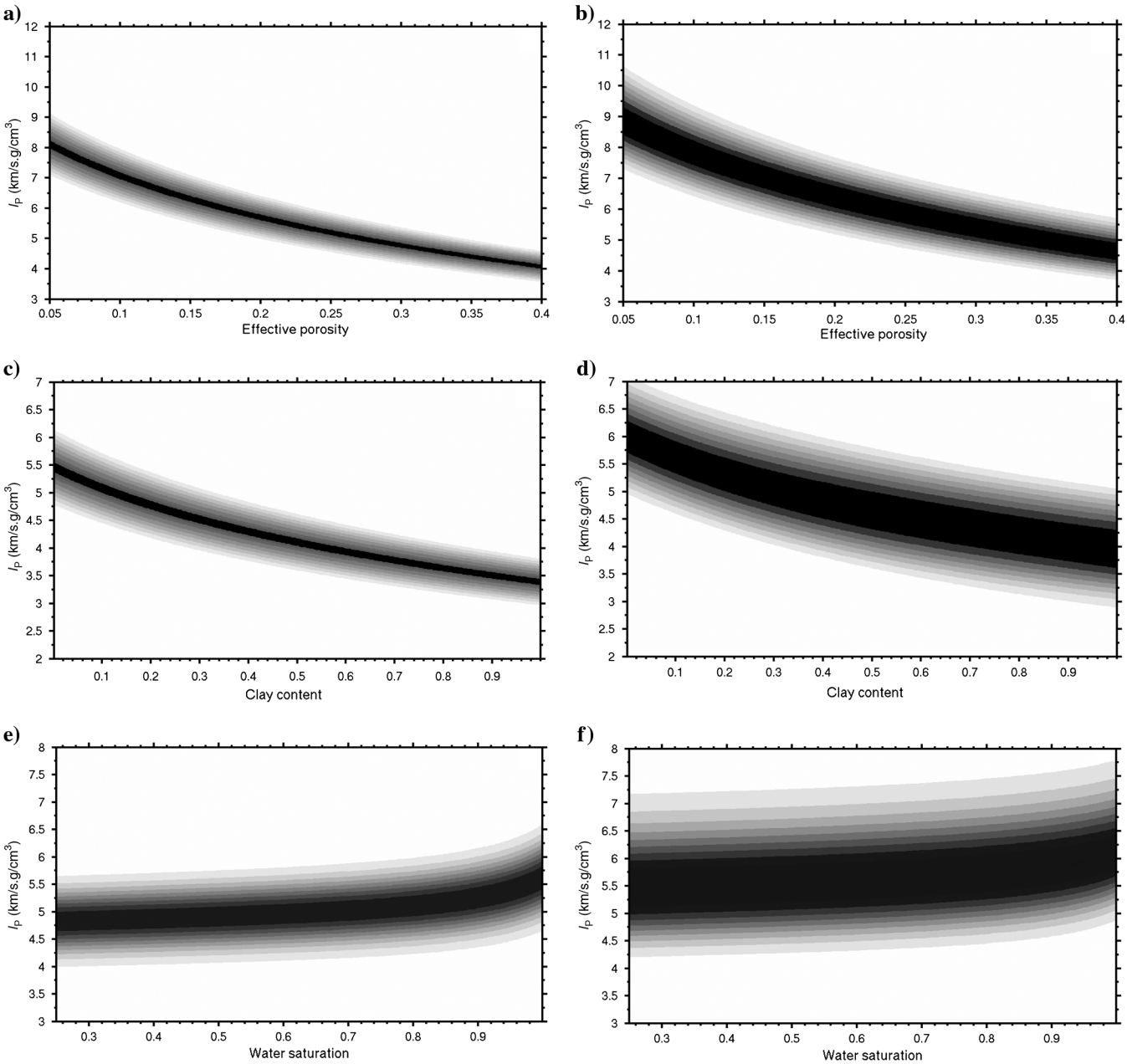

Figure 6. Uncertainty in the predictions of the petrophysical forward relations for I_P. (a) Plot of I_P versus porosity when other input parameters of the petrophysical forward relations are held constant. Ambiguity (gray area) is due to the overall effect of theoretical and measurement uncertainty. (b) Plot of I_P versus porosity when confounding parameters of the petrophysical forward function are varied. The thicker black and dark gray area show additional uncertainty due to variation of the confounding parameters. (c and d) Corresponding plots for I_P versus clay content. (e and f) Corresponding plots for I_P versus water saturation.

uncertainty in these three parameters. We could also do the same for any of the other parameters in the rock physics model.

Training data set and MDN specifications

The MDN input vector consists of the P- and S-wave-impedances $\mathbf{d} = (I_P, I_S)$, and its outputs are parameters of the mixture density model of the posterior PDF of the model vector $\mathbf{m} = (\phi_e, c, s_w)$. The output vectors of the training data set of the MDN were constructed by drawing samples from the a priori PDF of the model parameters, which are described in the a priori PDF section above. There were 846 equally spaced samples of porosity and clay content selected from the T-region in the ϕ_e-V_{cl} plane (Figure 4a). Forty equally spaced samples of s_w and six equally spaced samples of p_e were then selected from the intervals [0,1] and [173 bar , 332 bar], respectively. The values of the bulk modulus and density of each type of hydrocarbon were derived from the selected values of p_e to model the elastic behavior of the hydrocarbon (Figure 5). The total number of model vectors constructed in this way was 642,960.

The MDN will interpolate the relationship between **d** and **m** after training. To reduce the interpolation error of the MDN for the desired model parameters (ϕ_e, V_{cl}, s_w) we select samples from these parameters densely (i.e., $\Delta\phi_e = 0.009$, $\Delta V_{cl} = 0.0204$, and $\Delta s_w = 0.025$). Because the effect of confounding model parameters (p_e, K_{hc}, ρ_{hc}, K_w, ρ_w) is integrated out by the MDN, we select a smaller number of samples from these parameters and apply the MDN to interpolate and integrate the effect of other values. A denser sample selection of the above parameters will improve the accuracy of the MDN; however, it will increase the training time significantly.

For each of the 642,960 a priori model vectors selected above, one data vector (I_P, I_S) was calculated using the petrophysical forward relations. Three samples of Gaussian noise with zero mean were added to each of these data vectors to represent data uncertainty. The covariance matrix of Gaussian noise was equal to the sum of the measurement and theoretical uncertainty covariance matrices given in the forward modeling section above. The number of noisy model-data pairs derived in this way was therefore $3 \times 642,960 = 1,928,880$, which were used as the training data set.

The number of required kernels (equation A-1), and hidden units of the MDN were selected using a trial and error procedure (Shahraeeni and Curtis, 2009, 2011). Here, we describe the trial and error procedure. Four networks with different number of kernels and hidden units were trained for 100 iterations. Then error of each network over the well-log samples (validation error) was measured and the network with the minimum validation error was selected to continue the training procedure. In Table 1, a summary of training and validation errors of the four different networks is given. Overfitting of the network to the training data set (a source of instability in trained neural networks — Bishop [1995]) is controlled using the noisy training data set (Bishop, 1995, p. 346–349). Also, the total number of weights (free parameters of the network) is 2041, which is far smaller than the number of training samples and reduces the probability of overfitting significantly according to Vapnik and Chervonenkis theorem (Bishop, 1995, p. 377–380).

RESULTS

Inversion of Backus-averaged I_P and I_S well logs

In the first step of inversion, the Backus-averaged (Backus, 1962; Mavko et al., 2009) P- and S-wave impedance logs are inverted for porosity, clay content, and water saturation. Backus-averaged P- and S-wave impedance logs can be used as low-frequency estimates of P- and S-wave impedance logs. To evaluate results of petrophysical inversion of Backus-averaged P- and S-wave impedance, these results can be compared with measured petrophysical well logs.

To have the same frequency content as seismic data, we select a Backus averaging window equal to one-fourth of seismic

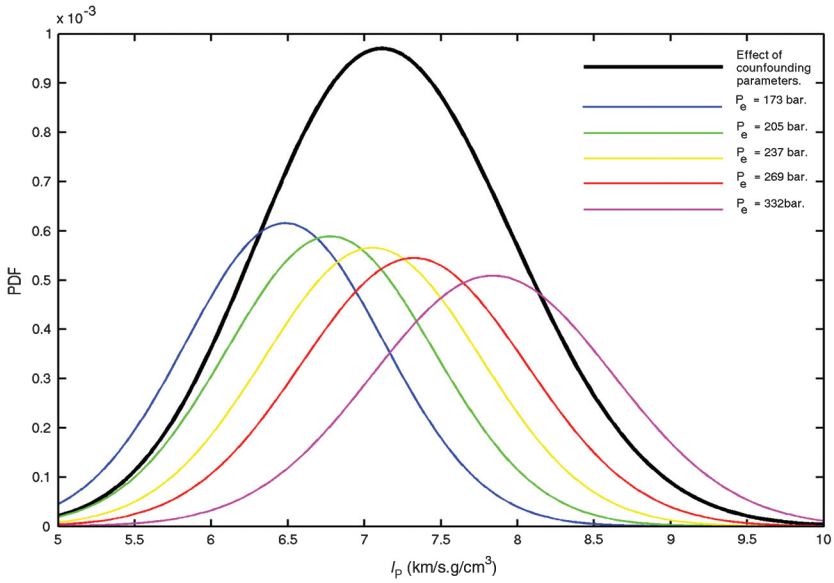

Figure 7. Uncertainty in I_P for different values of effective pressure (colored curves). The black curve is total uncertainty due to uncertainty in effective pressure as a confounding model parameter.

Table 1. Variation of the training and validation error due to different choices of the MDN's parameters.

Number of kernels	Number of hidden units	Normalized training error	Normalized validation error
5	52	−0.87	−0.73
	80	−0.89	−0.74
10	27	−1.00	−0.90
	40	−1.05	−0.90

wavelength. The average seismic wave frequency in the seismic data in this application is around 20 Hz and the average wave speed is around 2800 m/s, henceforth the wavelength is around 140 m. This wavelength is much larger than the typical thickness of layers in the well (at most 4 m) and, therefore, Backus averaging can be used to estimate the behavior of seismic wave. The Backus averaging window used was approximately one-fourth of the above seismic wavelength, which is around 35 m. Figure 8a and 8b shows the measured and Backus-averaged I_P and I_S for one well.

For the inversion of the Backus-averaged I_P and I_S logs, uncertainty of data was assumed to be equal to the uncertainty of the petrophysical forward function (Appendix A), and a priori information about model parameters was assumed to be the same as those described in the method section above. Another training data set was constructed using the same procedure as explained above.

We trained a separate MDN with the above data set and applied it to invert Backus-averaged I_P and I_S logs to obtain the a posteriori PDF of porosity, clay content, and water saturation logs. The results are shown in Figure 8c, 8d, and 8e, for porosity, clay content, and water saturation, respectively. Note that a relatively large bias in the value of clay content can be observed on the 3540–3640 ms interval. Figure 1 shows that the predictions of the petrophysical forward function are also biased on this interval. This observation means that applying the petrophysical forward function for inversion can result in large errors on the aforementioned interval.

Inversion of seismic I_P and I_S

The MDN with the specifications given above was trained using the training data set $\{(\mathbf{m}_k, \mathbf{d}_k) : k = 1, \ldots, NR\}$ to estimate the joint PDF of model vector $\mathbf{m} = (\phi_e, c, s_w)$ from data vector $\mathbf{d} = (I_P, I_S)$. In this section, we present results of the inversion of seismic I_P and I_S.

Figure 9 shows the joint marginal PDF's of model parameters evaluated at a randomly chosen data point at one well in the field with $I_P = 7345$ kg/(m^{2}s) and $I_S = 4658$ kg/(m^{2}s). The measured

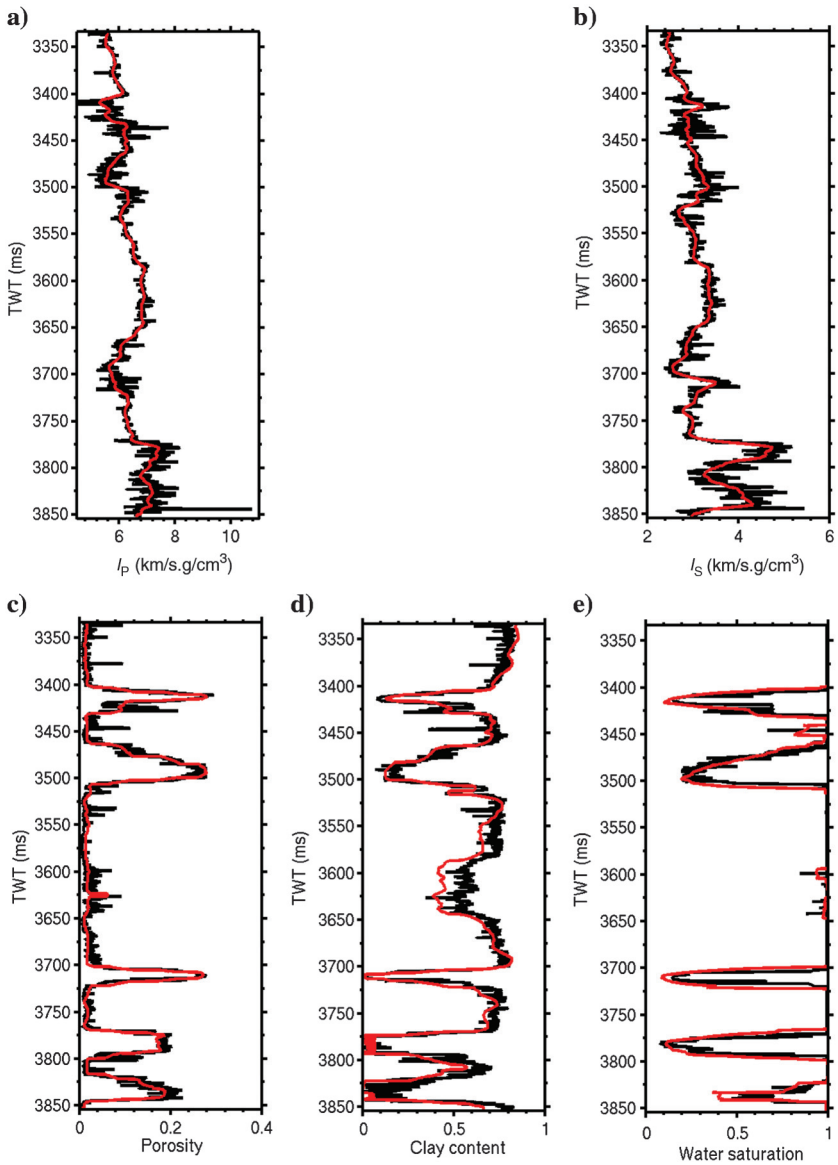

Figure 8. Comparison of the maximum a posteriori marginal PDF of petrophysical parameters obtained from inversion of the backus-averaged I_P and I_S logs and measured logs. (a) Measured I_P (black) and Backus-averaged I_P (red); (b) I_S. (c) Measured porosity (black) and inverted porosity (red). (d) Clay content. (e) Water saturation.

values of model parameters for this data point are $\phi_e = 0.19$, $c = 0.04$, and, $s_w = 0.13$, which are shown by crosses in Figure 9. The point estimates of porosity, clay content, and water saturation are obtained as the MAP points of the marginal PDF's and are equal to 0.17 for porosity, 0.04 for clay content, and 0.12 for water saturation.

To assess reduction of uncertainty in the model parameters after inversion, which is due to additional information in seismic data, we compare the posterior and the prior standard deviations. The standard deviation for the posterior PDF's of porosity, clay content, and water saturation are equal to 0.02, 0.05, and 0.17, respectively, while for the prior PDF's they are equal to 0.09, 0.26, and 0.30, respectively. The relative reduction in all three posterior standard deviations shows that the inversion process decreases the uncertainty of all model parameters. Remaining uncertainty in the model parameters is mainly due to uncertainty in effective pressure, other confounding parameters, theoretical uncertainty and error of the petrophysical forward relations, and error in I_P and I_S estimates obtained from seismic data. Note that, in general, reduction of uncertainty of water saturation is much smaller than reduction of uncertainty of porosity and clay content.

Figures 10 and 11 show the marginal PDF's of porosity, clay content, and water saturation, derived from the inversion of seismic I_P and I_S in two intervals along the well profile (performance at other wells is similar). The value of water saturation in these two intervals varies between 10% and 100%. The first rows in Figures 10 and 11 show results of the MDN inversion of seismic data. To assess the accuracy of the MDN solution, an MC sampling method was also applied to solve the same inverse problem on the above intervals. The a priori information about model parameters and the petrophysical forward relations used in the MC sampling inversion were the same as the MDN inversion. The marginal PDF's of the model parameters, which are obtained from MC sampling, are shown in the second row of Figures 10 and 11. Comparison between the results of the MDN inversion and MC sampling inversion shows that the MDN solution gives an acceptable approximation of the MC sampling solution. Shahraeeni and Curtis (2011) show other examples of the comparison between MC sampling and MDN inversion result. In those examples also, the MDN inversion results are acceptable estimates of MC sampling results. It can be argued that in some cases MDN results are better estimates of the low-resolution logs than MC sampling results; this might be due to the learning ability of neural networks.

In Figures 10 and 11, in addition to the marginal PDF's of the model parameters, a solid black line shows the result of inversion of Backus-averaged I_P and I_S. A solid red line shows the maximum a posteriori (MAP) of the marginal PDF's of the model parameters. Figures 10 and 11 show that the marginal PDF's of the model parameters derived from inversion of seismic I_P and I_S represent good estimates of the inversion result of Backus-averaged I_P and I_S. In particular, the MAP of the marginal PDF's (solid red lines in Figures 10 and 11) estimates the inversion result of Backus-averaged I_P and I_S with a reasonable accuracy. The difference between the values of porosity, clay content, and water saturation derived from seismic I_P and I_S and the values of these parameters derived as the MAP of the inversion of Backus-averaged I_P and I_S can be due to errors in the processing of the seismic data.

Figure 12a shows the MAP of porosity after inverting the I_P and I_S cross sections in Figure 3. Figure 12b shows the standard deviation of the marginal distribution of porosity in this cross section. The highest value of the color bar corresponds to the a priori standard deviation of porosity, and throughout the cross section the a posteriori standard deviation is smaller than this value (the color of the a priori standard deviation is red, and the hottest color in Figure 12b is light orange). Figures 13a and 14a show the MAP of clay content and water saturation, respectively, after inverting I_P

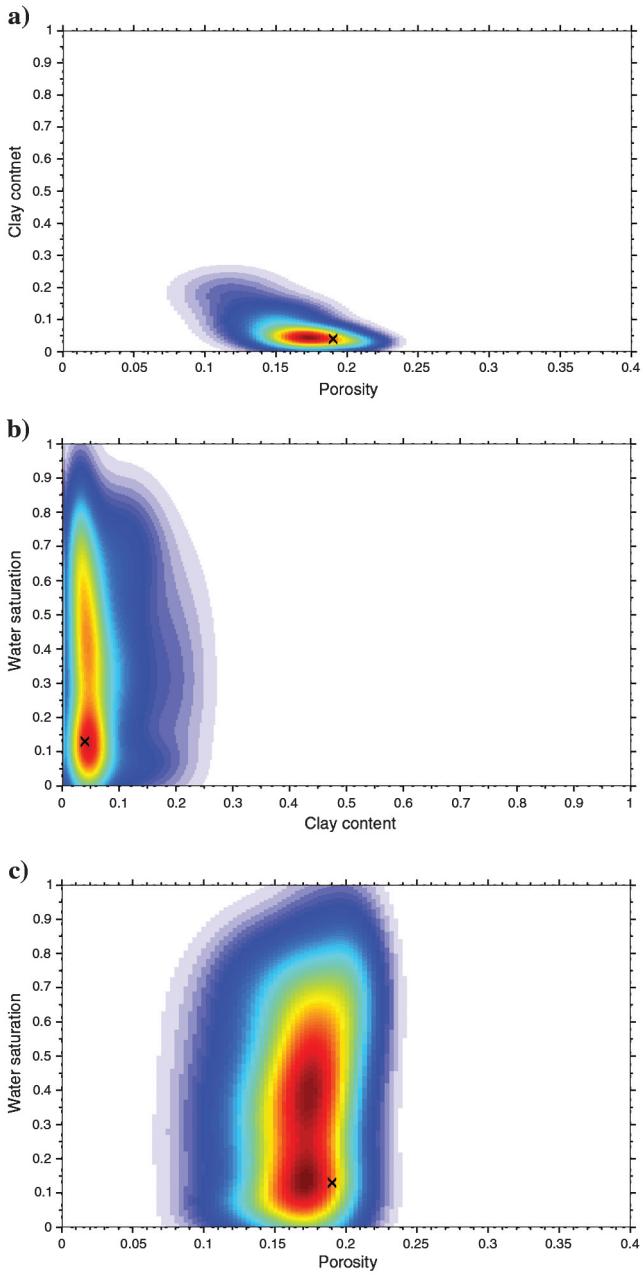

Figure 9. Marginal a posteriori joint PDF of model parameters for $I_P = 7345$ (km/s).(g/cm^3) and $I_S = 4658$ (km/s).(g/cm^3). (a) Marginal joint PDF of effective porosity and clay content. (b) Marginal joint PDF of clay content and water saturation. (c) Marginal joint PDF of effective porosity and water saturation. Hot colors show high probability zones. The black cross is the value of logs for this data point.

and I_S sections in Figure 3. Figures 13b and 14b show the standard deviations of clay content and water saturation in each section. Again, the highest values of the color bars correspond to the a priori standard deviation values, and it is evident that for all data points the a posteriori standard deviation is smaller than this value.

Figure 15 shows the MAP of model parameters for 30 neighboring traces of the well in the inline section perpendicular to the previous crossline section. Figures 12, 13, and 14, in addition to Figure 15 show this method gives a good 3D estimate of the underground rock and fluid properties. As indicated previously, in addition to the MAP and standard deviation estimate of the model parameters, any other statistical property of the model parameters can be calculated from the estimated conditional joint PDF $p(\phi_e, c, s_w|I_P, I_S)$, for any location spanned by the 3D seismic data sets.

DISCUSSION

Figures 10 and 11 show that the MAP's of the marginal a posteriori PDF of the model parameters are reasonable estimates of the values obtained from the inversion of the Backus-averaged logs. The error in the petrophysical inversion of seismic I_P and I_S can be related to uncertainty in the inverted seismic data and the accuracy of the petrophysical forward relations.

Figure 1 shows the measured well log of I_P and I_S and corresponding predictions of the petrophysical forward relations. Large biases in the predictions of the petrophysical forward relations can be seen in the interval 3550–3700 ms. These biases result in errors in the estimated values of porosity, clay content, and water saturation obtained from inversion of Backus-averaged I_P and I_S in Figure 8. In particular, we can see biases in the estimated clay content value on the same interval in that figure. The error over the above interval shows the effect of the accuracy of the petrophysical forward relations on the petrophysical inversion result. Appendix B shows that Reuss average of the elastic moduli of sand and shale and Gassmann theory are applied to derive the petrophysical forward function. The Reuss average is a lower bound of the elastic moduli of a mixture of rocks; therefore, the petrophysical forward function may underestimate the equivalent elastic moduli of the mixture of sand and shale. Application of more accurate theoretical models might improve the accuracy of the petrophysical forward function and reduce error in the petrophysical inversion result.

Figure 16a and 16b shows I_P and I_S obtained from seismic data and compare it with Backus-averaged logs for the two intervals in Figures 10 and 11. This figure shows that seismic inversion for I_S in the interval 3425–3470 ms has large errors (in some

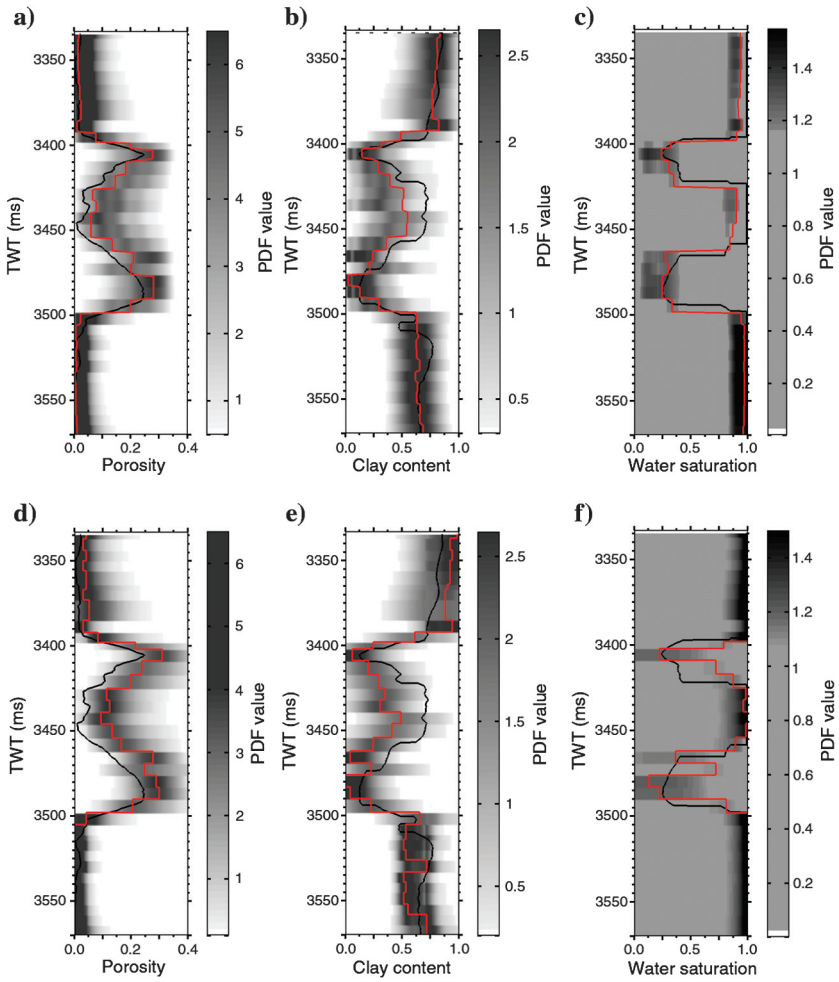

Figure 10. Marginal a posteriori PDF's of the model parameters from the inversion of seismically derived I_P and I_S for the depth interval 3335–3555 ms, in one of the wells. First row is the marginal PDF of the model parameters obtained using MDN: (a) Porosity ($R = 0.86$). (b) Clay content ($R = 0.80$). (c) Water saturation ($R = 0.84$). Second row is the joint PDF of the model parameters using MC sampling: (d) Porosity ($R = 0.86$). (e) Clay content ($R = 0.80$). (f) Water saturation ($R = 0.84$). Solid black line is the low-resolution log. Darker areas show high probability zones. The solid red line is the maximum a posteriori (MAP) of the marginal PDFs; R in each item shows the correlation coefficient between the MAP and low-resolution log.

cases near 25%, around two times larger than the 14% error used in the MDN inversion above). This error results in large errors in the inverted values of porosity and clay content on the same interval in Figure 10a and 10b. We also see large errors in the inverted values of I_P in the shale interval 3500–3550 ms, which result in errors in the inverted values of clay content on the same interval in Figure 10b. The errors in the above intervals show the effect of the accuracy of the processed seismic data on the petrophysical inversion result. Any improvement in the accuracy of the inverted seismic data can reduce the effect of this type of error.

The MDN inversion method relies on the validity of the seismic impedance inversion. Due to several sources of uncertainty such as wavelet parameters, seismic-to-well tie, low-frequency a priori impedance model, and amplitude processing, the seismic inversion can be biased and inaccurate away from the well. However, due to time efficiency of the MDN inversion method, it is possible to apply this method with multiple realizations of I_P and I_S obtained by probabilistic inversion of seismic data. In such cases, for each realization, the MDN gives the joint PDF of the petrophysical parameters. The average of these PDF's can be used as a petrophysical model that captures uncertainties due to uncertainties in the elastic inversion process.

Figures 9, 10, and 11 show the a posteriori uncertainty of porosity, clay content, and water saturation is large. The high uncertainty of model parameters stems from uncertainty about confounding model parameters (i.e., effective pressure, bulk modulus, and density of hydrocarbon), uncertainty of the petrophysical forward relations, and measurement uncertainty in seismic I_P and I_S. In addition of course, we invert only two data for three parameters, and hence, simply by appealing to dimensionality arguments, a unique solution is impossible without strong a priori information. Figures 6 and 7 show the effect of theoretical and measurement uncertainty in addition to the effect of the confounding model parameters on the uncertainty of I_P (the behavior of I_S is similar). In particular, for water saturation, in Figure 6f, we observe that uncertainty in the confounding model parameters results in large uncertainty in I_P values. Figure 6f shows that even when porosity and clay content values are known, for a given value of I_P the uncertainty of water saturation is large. This means that the reduction in uncertainty in the water saturation from the petrophysical inversion will always be small (Figures 9, 10, and 11). Bachrach (2009) and Spikes (2007) report the same high uncertainty for a posteriori water saturation in petrophysical inversion. Nevertheless, the inversion process does reduce the uncertainty of all model parameters as can be seen in Figures 12b, 13b, and 14b.

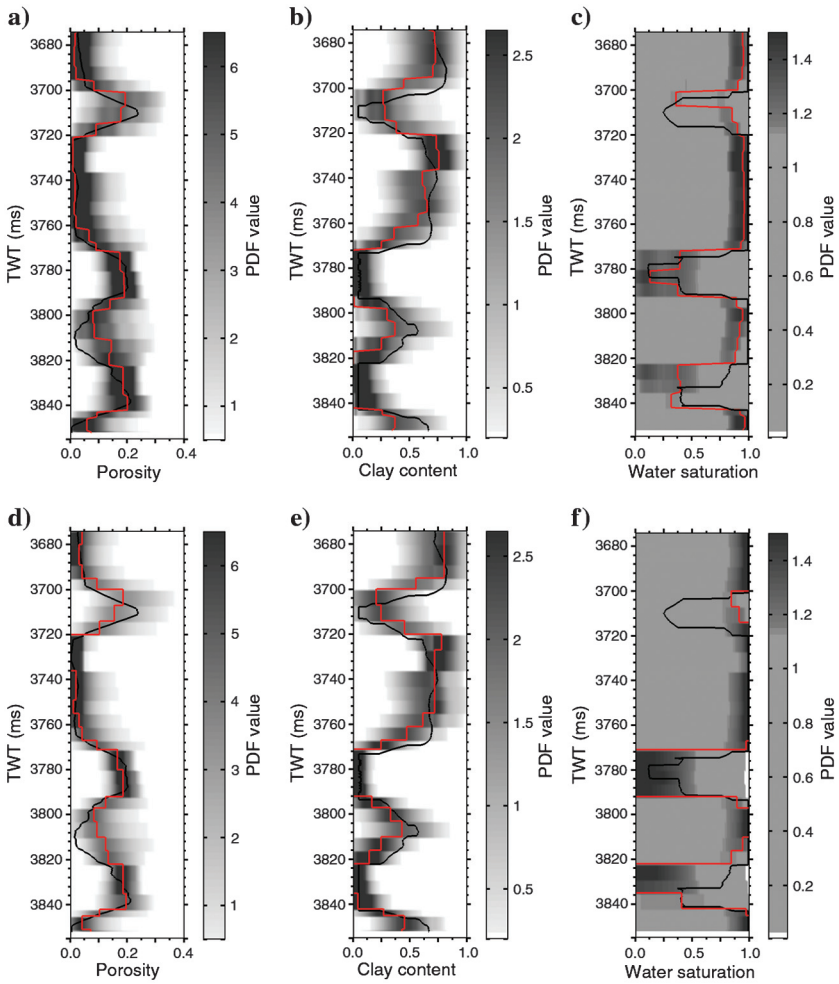

Figure 11. Marginal a posteriori PDFs of the model parameters from the inversion of seismically derived I_P and I_S for the depth interval 3674–3855 ms in one of the wells. First row is the marginal PDF of the model parameters obtained using MDN: (a) Porosity. (b) Clay content. (c) Water saturation. Second row is the joint PDF of the model parameters using MC sampling: (d) Porosity. (e) Clay content. (f) Water saturation. Solid black line is the low-resolution log. Darker areas show high probability zones. The solid red line is the maximum a posteriori (MAP) of the marginal PDF's. Correlation coefficients between low-resolution logs and MAP estimates are the same as those shown in Figure 10.

Figures 12a, 13a, and 14a in conjunction with Figure 15 show that if this method is applied to invert 3D seismic I_P and I_S sections, the estimates of porosity, clay content, and water saturation can provide a detailed 3D description of rock properties in a reservoir. This is of great value and importance for exploration and reservoir development plans as it can help to locate possible sources of hydrocarbon inside a reservoir. The accuracy and resolution of this description depends on the accuracy and resolution of 3D seismic impedance cubes, and on the accuracy of the petrophysical relationships used.

In some reservoirs, it is possible to observe rocks with different petrophysical properties (i.e., porosity and clay content) and similar values of I_P and I_S (Shahraeeni and Curtis, 2011). In such cases, due to multimodal nature of a posteriori PDF of the petrophysical properties, applying conventional fast probabilistic inversion methods (e.g., linearized inversion with Gaussian assumption about prior and posterior uncertainties [Rimstad and Omre, 2010]) can result in large errors in the estimated value of porosity and clay content. Shahraeeni and Curtis (2011) show that in those cases MDN can estimate the a posteriori PDF of the petrophysical parameters with acceptable accuracy. Also, we must note that the technique presented by Rimstad and Omre (2010) is very efficient and useful for integration of geological prior information in the petrophysical inversion procedure.

Due to large uncertainty associated with data, petrophysical forward relations, and confounding model parameters, the a posteriori PDF of model parameters, and especially water saturation will always have large uncertainty. To address this uncertainty appropriately, any petrophysical inversion method must be probabilistic. The MDN method is a time- and memory-efficient method for probabilistic nonlinear inversion. The nonlinear inversion of each crossline section, which included 170,322 data points and resulted in the full joint posterior PDFs of ϕ_e, c, and s_w, only took 340 s on a regular desktop computer. The number of crossline sections is 1461, so inverting the whole 3D seismic cube with 248,840,442 data points takes only around 138 hours on the same desktop computer. Note that solving the same number of petrophysical inverse problems using the MC sampling method will take around 27,500 hours on the same desktop computer (nearly 200 times more than MDN). What is more, the mixture density neural network encoded the full joint PDF of all model parameters for all data points into only 2041 scalar values (i.e., the number of MDN weights), which requires 20.5 KB memory for storage. The storage of the MC sampling results requires 3.2 MB, which means

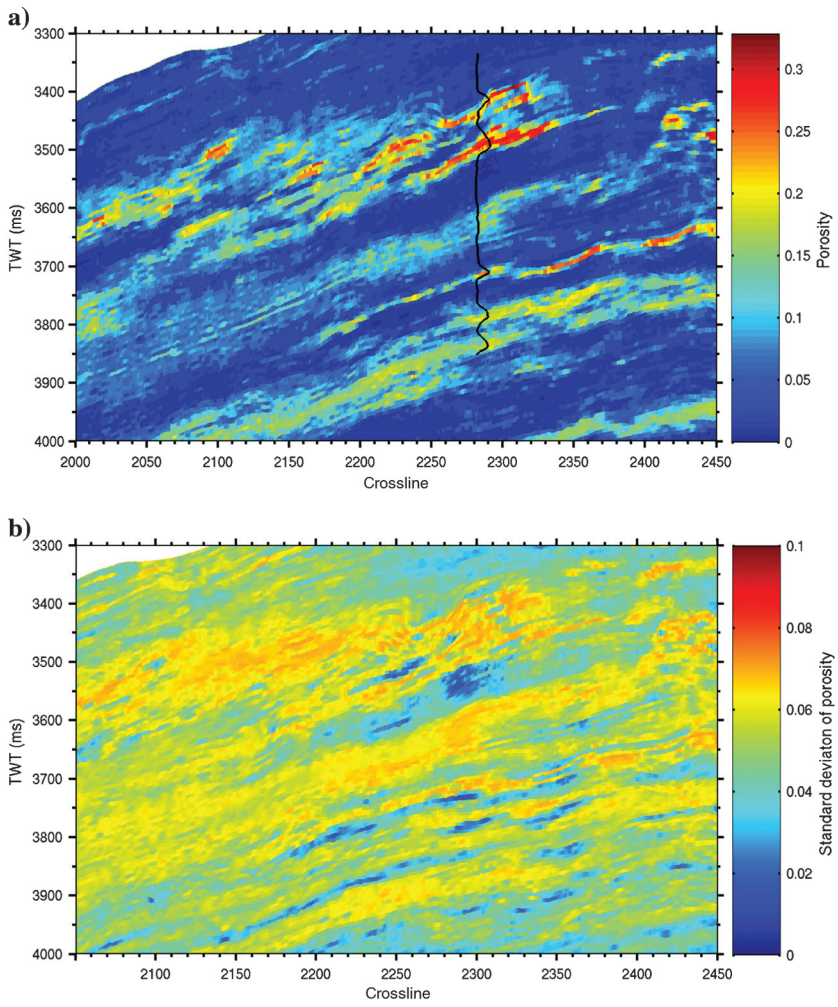

Figure 12. Estimated porosity and its associated uncertainty for one section from the seismic cube, which includes one of the wells. (a) Maximum a posteriori of the marginal PDF of porosity. (b) Standard deviation of porosity. The black line represents the upscaled well log.

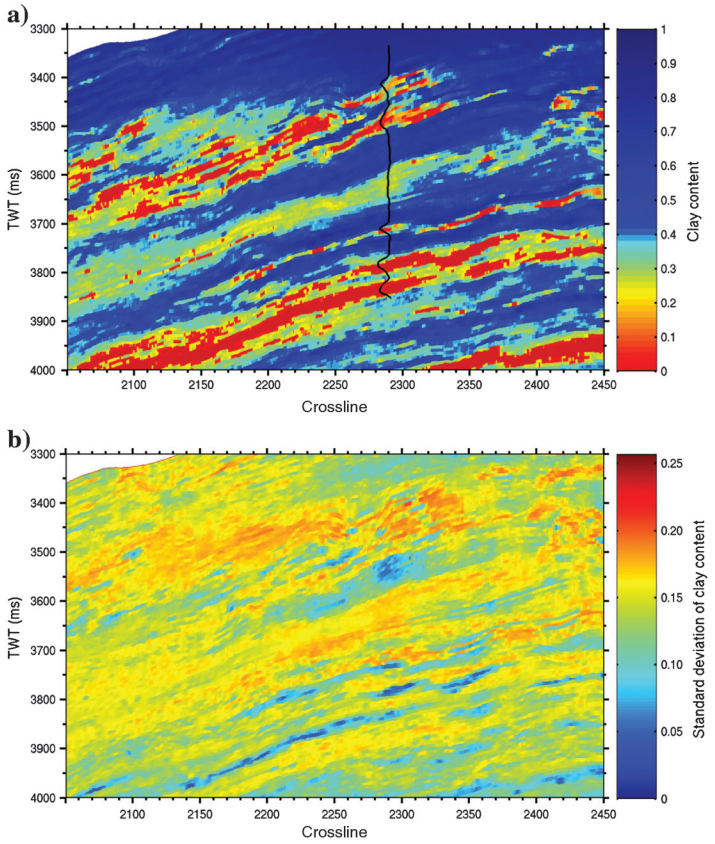

Figure 13. Estimated clay content and its associated uncertainty for one section from the seismic cube, which includes one of the wells. (a) Maximum a posteriori of the marginal PDF of clay content. (b) Standard deviation of clay content. The black line represents the upscaled well log.

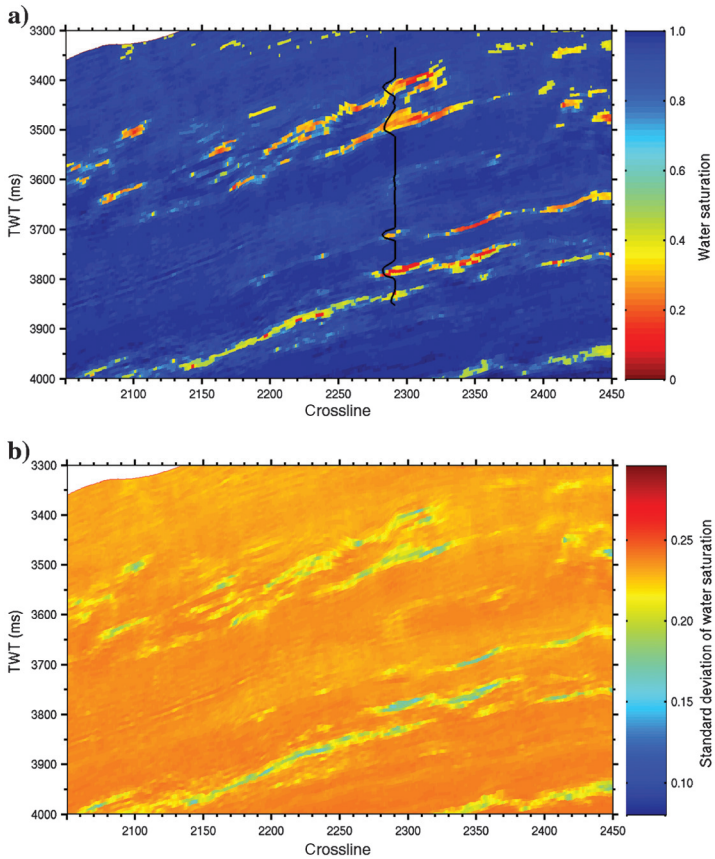

Figure 14. Estimated water saturation and its associated uncertainty for one section of the seismic cube, which includes one of the wells. (a) Maximum a posteriori of the marginal PDF of water saturation. (b) Standard deviation of water saturation. The black line represents the upscaled well log.

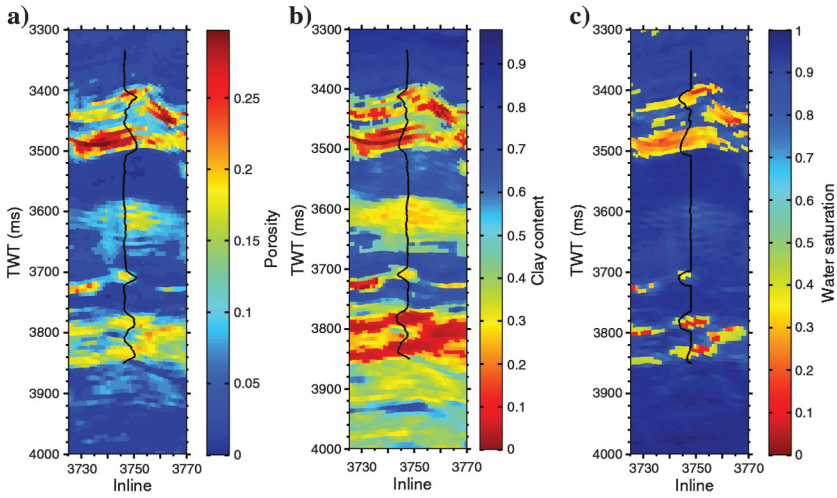

Figure 15. Estimated model parameters around the well in the inline section. (a) Porosity. (b) Clay content. (c) Water saturation. The black line represents the upscaled well log.

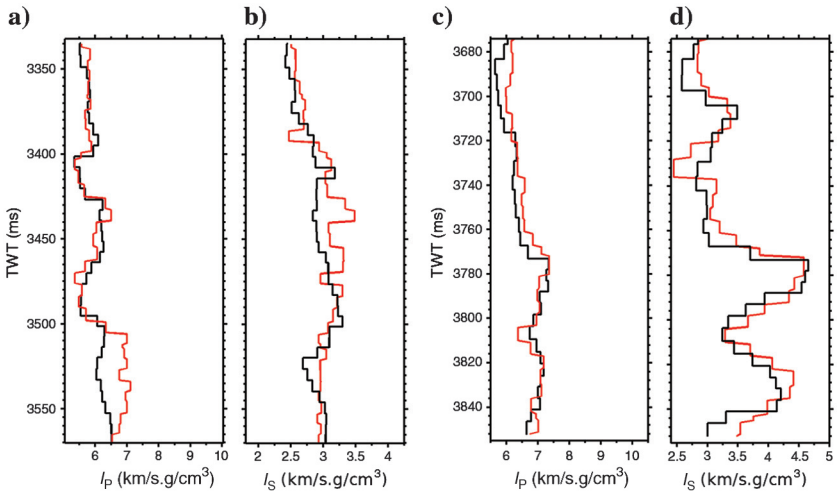

Figure 16. Comparison between seismically derived I_P and I_S (red) and upscaled measured logs (black). (a and b) are for the depth interval 3333–3570 ms. (c and d) are for the depth interval 3674–3855 ms. Correlation coefficients are given in Figure 3.

that for all data points around 2.4 TB (2.4×10^{12} Bytes) of memory is required. Using conventional inversion methods such as MC sampling to invert 3D seismic cubes is thus possible only when large parallel computing resources are available. On the other hand, the MDN inversion method is a fully probabilistic, non-Gaussian, nonlinear, petrophysical inversion method that is applicable to large seismic cubes on a standard desktop computer.

We must consider that there is a trade-off between time and memory efficiency of the MDN inversion technique, and the accuracy of the a posteriori PDF of model parameters estimated by this technique (Shahraeeni and Curtis, 2011). An MDN with a larger number of kernels usually results in a smaller training and validation error (Table 1), however, the time required to train such a network increases exponentially with the number of kernels. Another drawback of using MDN is that the selection of the number of kernels and hidden units is a trial and error procedure, which can take a long time. However, this time is usually much smaller than the time required for petrophysical inversion using the MC sampling method.

CONCLUSIONS

A fast probabilistic inversion method based on mixture density neural networks has been applied to jointly invert compressional and shear-wave impedances for the joint probability density function (PDF) of porosity, clay content, and water saturation in a 3D seismic cube. The inversion results at a well location show that the maximum a posteriori (MAP) of the marginal PDF's of the model parameters is a reasonable estimate of corresponding low-resolution log. Residual errors correspond to errors in the petrophysical forward relations, and differences between the seismic I_P and I_S and measured logs at wells. The uncertainty in the a posteriori PDF of the model parameters and in particular water saturation is high. This high uncertainty is related to presence of measurement uncertainty in I_P and I_S and also uncertainty about confounding model parameters. Nevertheless, the inversion process reduces the a priori uncertainty of all model parameters.

The result of the inversion gives a detailed description (to within the seismic resolution) of rock and fluid properties in the reservoir

that can be used for exploration and development planning. In particular, it can be used to find areas with high effective porosity and low clay content (pay zones), and also areas with possible sources of hydrocarbon based on the estimated water saturation.

The advantages of the mixture density neural network inversion method over other probabilistic inversion methods are its memory and computational efficiency. Due to the large size of 3D seismic cubes, these two properties are essential for any nonlinear probabilistic petrophysical inversion. As the inversion method is independent of the particular seismic attributes chosen in this case study (I_P and I_S), it can be used to invert any set of pertinent seismic attributes such as compressional- and shear-wave velocity and bulk density, or compressional impedance and Poisson's ratio. The main drawback of using MDN is the trial and error procedure of selecting the number of kernels and hidden units.

ACKNOWLEDGMENTS

We would like to thank TOTAL E&P UK for sponsoring this work. We acknowledge the support from the Scottish Funding Council for the joint research institute with the Heriot-Watt University, which is a part of Edinburgh Research Partnership in Engineering and Mathematics (ERPEM).

APPENDIX A

MIXTURE DENSITY NETWORK

One application of neural networks is to estimate some given mapping from an input vector $\mathbf{x}$ to a target vector $\mathbf{t}$. Any uncertainty associated with the target vector in this mapping can be represented by the probability density of $\mathbf{t}$ conditioned on (or given) $\mathbf{x}$, written as $p(\mathbf{t}|\mathbf{x})$. The MDN is a type of neural network that can be trained to emulate an approximation to $p(\mathbf{t}|\mathbf{x})$. Within the MDN, $p(\mathbf{t}|\mathbf{x})$ is represented by a mixture or sum of known probability densities:

$$p(\mathbf{t}|\mathbf{x}) = \sum_{i=1}^{m} \alpha_i(\mathbf{x})\varphi_i(\mathbf{t}|\mathbf{x}). \tag{A-1}$$

In equation A-1, $\varphi_i(\mathbf{t}|\mathbf{x})$ is a known PDF called a kernel, m is the number of kernels, and $\alpha_i(\mathbf{x})$ is the mixing coefficient that defines the weight of each kernel in the mixture (the sum). This representation of the PDF is called a mixture model.

A mixture of densities with Gaussian kernels can approximate any PDF to any desired accuracy, given a sufficient number of kernels with appropriate parameters (Shahraeeni and Curtis, 2011). We assume kernels are Gaussian with a diagonal covariance matrix:

$$\varphi_i(\mathbf{t}|\mathbf{x}) = \frac{1}{\prod_{l=1}^{c}\left(\sqrt{2\pi}\,\sigma_{il}(\mathbf{x})\right)} \exp\left\{-\frac{1}{2}\sum_{l=1}^{c}\frac{(t_l-\mu_{il}(\mathbf{x}))^2}{\sigma_{il}^2(\mathbf{x})}\right\}, \tag{A-2}$$

where c is the dimensionality of the output vector $\mathbf{t} = (t_1, \ldots, t_c)$, $\mu_{il}(\mathbf{x})$ is the lth component in the mean vector of the ith kernel, and σ_{il} is the lth diagonal element in the covariance matrix of the ith kernel. Therefore, the mean and covariance of the ith Gaussian kernel are $\boldsymbol{\mu}_i = (\mu_{i1}, \ldots, \mu_{ic})$, and $\boldsymbol{\Sigma}_i = \mathrm{diag}(\sigma_{i1}^2, \ldots, \sigma_{ic}^2)$, respectively.

Appropriate values for the parameters of the MDN (i.e., mixing coefficients, mean and covariance matrix of kernels) in equations A-1 and A-2 can be predicted by using any standard neural network (Bishop, 1995). We apply a two-layer feed-forward neural network with a single hidden layer of hyperbolic tangent functions and an output layer of linear functions.

In the network training phase, n statistically independent pairs of example input and output vectors $\{\mathbf{x}_j, \mathbf{t}_j\}$ are used as training samples. Unknown parameters of the network, which are referred to as weights, are determined in such a way that the likelihood of the training samples with respect to the density function in equation A-1 is maximized. The maximization of the likelihood is equivalent to minimization of the error function E, defined as

$$E = \sum_{j=1}^{n} E_j = -\sum_{j=1}^{n} \ln\, p(\mathbf{t}_j|\mathbf{x}_j). \tag{A-3}$$

To find the minimum of E, an optimization algorithm called scaled conjugate gradient is used. This algorithm determines the minimum of E with respect to the weights of the network, iteratively. In each iteration the algorithm requires derivatives of E with respect to the network weights, which are derived by using the so-called back-propagation algorithm (see Bishop (1995) for an explanation of the optimization and back-propagation algorithms).

Shahraeeni and Curtis (2011) show two examples of MDN solution of inverse problems and compare results with Monte Carlo (MC) sampling solution. Their results show that MDN can estimate MC sampling solution with an acceptable accuracy.

APPENDIX B

PETROPHYSICAL FORWARD RELATIONS

The petrophysical forward function is a set of mathematical equations that links the petrophysical parameters of a rock to its elastic parameters (i.e., P- and S-wave velocity and density). Many parameters can have an influence on the elastic parameters of a rock including porosity, size and shape of grains, clay content, fluid saturation, type of mineral matrix, sorting and arrangement of grains, effective pressure, temperature, burial, and history of the rock (i.e., diagenesis, tectonics, etc.). In this study, the approach to the petrophysical forward function construction is to explain the influence of these parameters on the elastic properties as much as possible.

In the field under study, we only observe turbidite sands within shaley intervals. In this field, shaley intervals are defined as intervals with clay volume larger than 60%, and effective porosity lower than 5%. First, we develop the petrophysical forward function for the shaley intervals. Shales are normally not cemented and silt grains are suspended in the clay matrix of shales (Avseth, 2005). In this case, Reuss average can be used to estimate the elastic moduli of shale layers:

$$K_{\mathrm{sh}} = \left(\frac{1-V_{cl}}{K_{\mathrm{qz}}} + \frac{V_{cl}}{K_{\mathrm{clay}}}\right)^{-1} \tag{B-1}$$

$$\mu_{\mathrm{sh}} = \left(\frac{1-V_{cl}}{\mu_{\mathrm{qz}}} + \frac{V_{cl}}{\mu_{\mathrm{clay}}}\right)^{-1} \tag{B-2}$$

In the above equations, V_{cl} is clay content, K_{qz} and μ_{qz} are bulk and shear moduli of silts, which are assumed to be mainly

composed of quartz, K_{clay} and μ_{clay} are the corresponding parameters of fluid saturated clay particles, and K_{sh} and μ_{sh} are the corresponding parameters of shales.

We applied the approach of Meadows et al. (2005) to model K_{clay} and μ_{clay} as empirical functions of effective porosity and effective pressure. We slightly modified the aforementioned approach by using effective porosity instead of total porosity. However, due to the fact that this approach is an empirical approach, this modification would not impose any additional error on the modeled elastic parameters of clay. Well-log data on the shaley intervals are applied to calibrate the empirical relationships. In this sense the petrophysical forward function is empirical.

Second, we develop the petrophysical forward function for sand intervals. In sand intervals, clay particles are assumed to be dispersed in the sand matrix and therefore total porosity can be represented as a function of effective porosity and clay content:

$$\phi = \frac{\phi_e}{1 - V_{cl}}. \tag{B-3}$$

In the above equation, ϕ is total porosity, and ϕ_e is effective porosity.

Following the approach of Nur et al. (1995), bulk and shear moduli of dry sand, K_{dry} and μ_{dry}, is modeled as

$$K_{dry} = K_{qz}\left(1 - \frac{\phi}{\phi_c}\right), \tag{B-4}$$

$$\mu_{dry} = \mu_{qz}\left(1 - \frac{\phi}{\phi_c}\right). \tag{B-5}$$

In the above equation, $\phi_c$is critical porosity. The ratio ϕ/ϕ_c is represented as an empirical function of effective pressure and porosity (Chao, 2009). The above empirical functions are calibrated with well-log data. Based on the available data at wells, the effect of other potentially influential parameters such as temperature or diagenesis is assumed to be negligible in this petrophysical forward function. The existence of such effects in some areas of the field will result in inaccurate predictions of the petrophysical forward function.

In this study, we assume that rocks are macroscopically homogenous, pores are interconnected, fluid is frictionless, and the rock-fluid system is closed. Therefore, Gassmann theory can be used to perform fluid substitution for different values of water saturation (Wang, 2001). Using the bulk and shear moduli of dry sand in equations B-4 and B-5, we obtain the following equations:

$$K_{sand} = K_{dry} + \left[1 - \frac{K_{dry}}{K_{qz}}\right]^2 \Big/ \left[\frac{\phi}{K_f} + \frac{(1-\phi)}{K_{qz}} + \frac{K_{dry}}{K_{qz}^2}\right], \tag{B-6}$$

$$\mu_{sand} = \mu_{dry}. \tag{B-7}$$

Here K_f is the bulk modulus of saturating fluid.

The pore fluid bulk modulus K_f is the bulk modulus of the mixture of water and hydrocarbon inside the effective pore space. By assuming a homogeneous mixture of water and hydrocarbon, this bulk modulus is obtained as

$$K_f = \left[\frac{S_W}{K_W} + \frac{1 - S_W}{K_H}\right]^{-1}. \tag{B-8}$$

In the above equation, S_W is water saturation, K_W is the bulk modulus of brine, and K_H is the bulk modulus of hydrocarbon. The interconnectivity of pores in shale is questionable, and therefore, application of Gassmann for them can result in errors. However, in this study we observe that the effect of this error can be neglected. More accurate petroelastic models might be used to model the behavior of shale and therefore reduce errors.

geologic observations at the well locations suggest that sand-shale mixtures in this field are mainly laminated. The petrophysical forward function for a laminated sand-shale mixture is derived by assuming that laminas are arranged perpendicular to the direction of wave propagation (Dvorkin and Gutierrez, 2001). For this arrangement, the bulk and shear moduli of sand-shale mixture are derived by Backus averaging of the bulk and shear moduli of sand and shale laminas:

$$K_{mix} = \left(\frac{1 - V_{cl}}{K_{sand}} + \frac{V_{cl}}{K_{shale}}\right)^{-1}, \tag{B-9}$$

$$\mu_{mix} = \left(\frac{1 - V_{cl}}{\mu_{sand}} + \frac{V_{cl}}{\mu_{shale}}\right)^{-1}. \tag{B-10}$$

Note that the above two equations are the Reuss average of elastic moduli of sand and shale laminas, which is a lower bound of the elastic moduli of laminas. Therefore, if the perpendicular wave incident assumption is violated in the laminated sand-shale mixture, application of the above formulas result in an underestimate of the equivalent elastic moduli of the mixture.

Assuming that the earth is isotropic and linearly elastic, the seismic behavior of sediments can be completely characterized by three parameters: bulk modulus, shear modulus, and bulk density. Bulk density ρ_{min} is calculated as the volumetric average of density of solid phase and liquid phase. The P- and S-wave impedances are derived from the bulk and shear moduli of saturated rock (equation B-9, B-10), and bulk density:

$$I_P = \sqrt{\rho_{mix}(K_{mix} + 4/3\mu_{mix})}, \tag{B-11}$$

$$I_S = \sqrt{\rho_{mix}\,\mu_{mix}}. \tag{B-12}$$

The above petrophysical forward relations are calibrated with data from eight wells in the field under study to construct the petrophysical forward function used in the inversion process.

Because the petrophysical forward function is calibrated on several wells, its uncertainty can be large. For high effective pressure (more than 100 bar) these uncertainties can be modeled by a Gaussian PDF with zero mean and standard deviation of 4% for I_P and of 6% for I_S (Chao et al., 2009).

REFERENCES

Aki, K., and K. P. G. Richards, 1997, Quantitative seismology: Theory and methods: University Science Books.

Avseth, P., T. Mukerji, A. Jorstad, G. Mavko, and T. Veggeland, 2001, Seismic reservoir mapping from 3-D AVO in a North Sea Turbidite system: Geophysics, **66**, 1157–1176, doi: 10.1190/1.1487063.

Avseth, P., T. Mukerji, and G. Mavko, 2005, Quantitative seismic interpretation: Applying rock physics tools to reduce interpretation risk: Cambridge University Press.

Bachrach, R., 2006, Joint estimation of porosity and saturation using stochastic rock-physics modeling: Geophysics, **71**, no. 5, O53–O63, doi: 10.1190/1.2235991.

Backus, G. E., 1962, Long-wave elastic anisotropy produced by horizontal layering: Journal of Geophysical Research, **67**, 4427–4440, doi: 10.1029/JZ067i011p04427.

Batzle, M., and M. Z. Wang, 1992, Seismic properties of pore fluids: Geophysics, **57**, 1396–1408, doi: 10.1190/1.1443207.

Bishop, C. M., 1995, Neural networks for pattern recognition: Oxford University Press.

Bosch, M., L. Cara, J. Rodrigues, A. Navarro, and M. Diaz, 2007, A Monte Carlo approach to the joint estimation of reservoir and elastic parameters from seismic amplitudes: Geophysics, **72**, no. 6, O29–O39, doi: 10.1190/1.2783766.

Bosch, M., C. Carvajal, J. Rodrigues, A. Torres, M. Aldana, and J. Sierra, 2009, Petrophysical seismic inversion conditioned to well-log data: Methods and application to a gas reservoir: Geophysics, **74**, no. 2, O1–O15, doi: 10.1190/1.3043796.

Bosch, M., T. Mukerji, and E. Gonzalez, 2010, Seismic inversion for reservoir properties combining statistical rock physics and geostatistics: A review: Geophysics **75**, no. 5, 75A165–75A176, doi: 10.1190/1.3478209.

Buland, A., O. Kolbjornsen, R. Hauge, O. Skjaeveland, and K. Duffaut, 2008, Bayesian lithology and fluid prediction from seismic prestack data: Geophysics, **73**, no. 3, C13–C21, doi: 10.1190/1.2842150.

Buland, A., O. Kolbjornsen, and H. Omre, 2003, Rapid spatially coupled AVO inversion in the Fourier domain: Geophysics, **68**, 824–836, doi: 10.1190/1.1581035.

Buland, A., and H. Omre, 2003, Bayesian linearized AVO inversion: Geophysics, **68**, 185–198, doi: 10.1190/1.1543206.

Chao, G., G. Lambert, and H. Cumming, 2009, Analysis of intrinsic uncertainties of petro-elastic models using simulated annealing: 71st EAGE Conference & Exhibition.

Devilee, R. J. R., A. Curtis, and K. Roy-Chowdhury, 1999, An efficient, probabilistic neural network approach to solving inverse problems: Inverting surface wave velocities for Eurasian crustal thickness: Journal of Geophysical Research, **104**, 28841–28857, doi: 10.1029/1999JB900273.

Doyen, P. M., 1988, Porosity from seismic data: A geostatistical approach: Geophysics, **53**, 1263–1275, doi: 10.1190/1.1442404.

Dubrule, O., 2003, Geostatistics for seismic data integration in earth models: SEG.

Dvorkin, J., and M. A. Gutierrez, 2001, Textural sorting effect on elastic velocities, Part II: Elasticity of a bimodal grain mixture: 71th Annual International Meeting, SEG, Expanded Abstracts, 1764–1767.

Eftekharifar, M., and D. Han, 2011, 3D petrophysical modeling using complex seismic attributes and limited well log data: 81th Annual International Meeting, SEG, Expanded Abstracts, 1887–1891.

Eidsvik, J., P. Avseth, H. Omre, T. Mukerji, and G. Mavko, 2004, Stochastic reservoir characterization using prestack seismic data: Geophysics, **69**, 780–993, doi: 10.1190/1.1778241.

Gonzalez, E. F., T. Mukerji, and G. Mavko, 2008, Seismic inversion combining rock physics and multiple-point geostatistics: Geophysics, **73**, no. 1, R11–R21, doi: 10.1190/1.2803748.

Grana, D., and E. Della Rossa, 2010, Probabilistic petrophysical-properties estimation integrating statistical rock physics with seismic inversion: Geophysics, **75**, no. 3, O21–O37, doi: 10.1190/1.3386676.

Hampson, D. P., J. S. Schuelke, and J.A. Quirein, 2001, Use of multiattribute transforms to predict log properties from seismic data: Geophysics, **66**, 220, doi: 10.1190/1.1444899.

Maiti, S., R. K. Tiwari, and H. J. Kumpel, 2007, Neural network modelling and classification of lithofacies using well log data: A case study from KTB borehole site: Geophysical Journal International, **169**, 733–746, doi: 10.1111/gji.2007.169.issue-2.

Maiti, S., and S. R. K. Tiwari, 2009, A hybrid Monte Carlo method based artificial neural networks approach for rock boundaries identification: A case study from the KTB bore hole: Pure and Applied Geophysics, **166**, 2059–2090, doi: 10.1007/s00024-009-0533-y.

Malinverno, A., and R. L. Parker, 2006, Two ways to quantify uncertainty in geophysical inverse problems: Geophysics, **71**, no. 3, W15–W27, doi: 10.1190/1.2194516.

Mavko, G., T. Mukerji, and J. Dvorkin, 2009, The rock physics handbook: Tools for seismic analysis of porous media: Cambridge University Press.

Meadows, M., D. Adams, R. Wright, A. Tura, S. Cole, and D. Lumley, 2005, Rock physics analysis for time-lapse seismic at Schiehallion field; North Sea: Geophysical Prospecting, **53**, 205–213, doi: 10.1111/gpr.2005.53.issue-2.

Meier, U., A. Curtis, and J. Trampert, 2007a, A global crustal model constrained by non-linearised inversion of fundamental mode surface waves: Geophysical Research Letters, **34**, L16304–L16304, doi: 10.1029/2007GL030989.

Meier, U., A. Curtis, and J. Trampert, 2007b, Global crustal thickness from neural network inversion of surface wave data: Geophysical Journal International, **169**, 706–722, doi: 10.1111/gji.2007.169.issue-2.

Meier, U., J. Trampert, and A. Curtis, 2009, Global variations of temperature and water content in the mantle transition zone from higher mode surface waves: Earth Planetary Science Letters, **282**, no. 1–4, 91–101, doi: 10.1016/j.epsl.2009.03.004.

Mukerji, T., A. Jorstad, P. Avseth, G. Mavko, and J. R. Granli, 2001, Mapping lithofacies and pore-fluid probabilities in a North Sea reservoir: Seismic inversions and statistical rock physics: Geophysics, **66**, 988–1001, doi: 10.1190/1.1487078.

Nur, A., G. Mavko, J. Dvorkin, and D. Gal, 1995, Critical porosity: The key to relating physical properties to porosity in rocks: 65th Annual International Meeting, SEG, Expanded Abstracts, 878–881.

Poulton, M. M., 2002, Neural networks as an intelligence amplification tool: A review of applications: Geophysics, **67**, 979–993, doi: 10.1190/1.1484539.

Rimstad, K., and H. Omre, 2010, Impact of rock-physics depth trends and Markov random fields on hierarchical Bayesian lithology/fluid prediction: Geophysics, **75**, no. 4, R93, doi: 10.1190/1.3463475.

Sambridge, M., and K. Mosegaard, 2002, Monte Carlo methods in geophysical inverse problems: Reviews of Geophysics, **40**, no. 3, 1009, doi: 10.1029/2000RG000089.

Schultz, P. S., S. Ronen, M. Hattori, and C. Corbett, 1994, Seismic-guided estimation of log properties, Parts 1, 2, and 3: The Leading Edge, **13**, 305, doi: 10.1190/1.1437020.

Sen, M. K., and P. L. Stoffa, 1991, Nonlinear one-dimensional seismic waveform inversion using simulated annealing: Geophysics, **56**, 1624–1638, doi: 10.1190/1.1442973.

Sengupta, M., and R. Bachrach, 2007, Uncertainty in seismic-based pay volume estimation: Analysis using rock physics and Bayesian statistics: The Leading Edge, **26**, 184–189, doi: 10.1190/1.2542449.

Shahraeeni, M. S., and A. Curtis, 2009, Nonlinear petrophysical inversion with mixture density neural networks: 71st EAGE Conference and Exhibition, Amsterdam.

Shahraeeni, M. S., and A. Curtis, 2011, Fast probabilistic nonlinear petrophysical inversion: Geophysics, **76**, no. 2, E45–E58, doi: 10.1190/1.3540628.

Spikes, K., T. Mukerji, J. Dvorkin, and G. Mavko, 2007, Probabilistic seismic inversion based on rock-physics models: Geophysics, **72**, no. 5, R87–R97, doi: 10.1190/1.2760162.

Tarantola, A., 2005, Inverse problem theory and methods for model parameter estimation: SIAM.

Tarantola, A., and B. Valette, 1982, Inverse problems = quest for information: Journal of Geophysics, **50**, no. 3, 159–170, doi: 10.1038/nrn1011.

Wang, Z. Z., 2001, Fundamentals of seismic rock physics: Geophysics, **66** , 398–412, doi: 10.1190/1.1444931.